Multiple Profiles Sensor-Based Monitoring and Anomaly Detection

Chen Zhang[1], Hao Yan[2], Seungho Lee[3], and Jianjun Shi[4]

[1]Tsinghua University, Beijing, 100084

[2]Arizona State University, Tempe, AZ, 85281

[3]Samsung Electronics, Suwon, South Korea, 443742

[4]Georgia Institute of Technology, Atlanta, GA, 30332

Abstract

Generally, in an advanced manufacturing system, hundreds of sensors are deployed to measure key process variables in real time. Thus, it is desirable to develop methodologies to use those real-time sensor data for on-line system condition monitoring and anomaly detection. However, there are several challenges in developing an effective process monitoring system: i) Data streams generated by multiple sensors are high-dimensional profiles; ii) Sensor signals are affected by noise due to system inherent variations; iii) Signals of different sensors have cluster-wise features; iv) An anomaly may only cause sparse changes of sensor signals. To address these challenges, this paper presents a real-time multiple sensor-based process monitoring system, which includes the following modules: (i) preprocessing sensor signals to remove inherent variations and conduct profile alignments, (ii) using

---

Dr. Zhang is an Assistant Professor in Department of Industrial Engineer at Tsinghua University. Her email is zhangchen@u.nus.edu .
Dr. Yan is an Assistant Professor in School of Computing, Informatics, Decision Systems Engineering at Arizona State University. His email is HaoYan@asu.edu .
Dr. Lee is a Principal Engineer in Samsung Electronics. His email is mountlee@gmail.com .
Dr. Shi is the Carolyn J. Stewart Chair and Professor in H. Milton Stewart School of Industrial and Systems Engineering at Georgia Institute of Technology. He is the corresponding author. His email is jianjun.shi@isye.gatech.edu .

multichannel functional principal component analysis (MFPCA) based methods to extract sensor features by considering cluster-wise between-sensor correlations, and (iii) constructing a monitoring scheme with the top-*R* strategy based on the extracted features, which has scalable detection power for different fault patterns. Finally, we implement and demonstrate the proposed framework using data from a real manufacturing system.

Keywords: Data fusion; Functional PCA; Multichannel profile monitoring; Statistical process control

1. Introduction

Advanced automatic data collection and inspection technologies have been widely adopted in manufacturing nowadays, which generate large amounts of high-dimensional data streams from multiple sensors characterizing the process. Those multiple sensor data provide opportunities for on-line process monitoring and anomaly detection. However, several challenges should be addressed to develop such an on-line monitoring system.

The first and the most crucial challenge is how to process high-dimensional, cross-correlated streaming data. These high-dimensional data streams lead to a large number of process parameters to be estimated and consequently require a very large in-control (IC) reference sample size. However, only limited reference samples can be gathered in a manufacturing process. When the data dimension is larger than the reference sample size, we will face the curse of dimensionality: it is prohibitive to estimate the joint process distribution, or even its covariance matrix, with limited reference samples. Then traditional multivariate SPC methods, such as the Hotelling T^2 chart, will become infeasible. This triggers high demand for new SPC methods.

The second challenge is that multiple variation patterns exist in a manufacturing process. For example, if the process is self-controlled, sensor signals of different products (samples) may be unsynchronized and have different time lengths due to sample-to-sample variations. Meanwhile, the manufacturing

equipment may undergo long-term drifts: sensor signals of the first and the consequent products may be at different levels even though all the products are within the pre-specified tolerances, i.e., in control. As such, we need to consider how to preprocess raw sensor signals to remove these system inherent variations for accurate comparison and analysis.

The third challenge is that a complicated correlation structure exists typically among high-dimensional streaming data. First, data produced by each sensor are nonstationary and strongly auto-correlated, which can be regarded as profile (functional) data with within-sensor (within-profile) correlations over time. Since traditional SPC schemes assume that the collected data are independent and identical distributed (*i.i.d*), these SPC schemes cannot be applied here directly. Second, on the one hand, sensors from the same source may have similar features, i.e., be cross-correlated. Although monitoring each sensor separately could reduce data dimensionality, this method neglects sensor cross-correlations and will eventually sacrifice the detection power. In other words, while separate monitoring might be still useful for detecting change patterns occurred in each single sensor profile, this method is ineffective in detecting changes of sensor cross-correlations. On the other hand, sensor profiles from different sources can show quite different features. Since different data features require particularly tailored analysis methods, different control charts should be designed separately to fit different data features. Therefore, it may be suboptimal if we directly monitor all sensors jointly using one unique control chart without considering data feature difference. With this in mind, we need to strike a balance between separate and joint monitoring of multiple sensor profiles.

The last but not the least challenge is that only a small number of sensor profiles will be influenced or shifted when the manufacturing process goes out of control. Since the influenced sensors or signals are sparse among the high-dimensional process data, it increases the challenges in change detection. Monitoring all sensor profiles without an effective sensor selection technique may result in detection power losses.

In summary, it is a challenging task to design a unified scheme to monitor multiple sensor profiles. This paper will address those challenges and develop a monitoring system. The following subsections will provide a motivation example, literature review, and a summary of our contributions.

1.1 A Motivation Example

We use real sensor data from an advanced manufacturing process as an example to illustrate the aforementioned challenges. The manufacturing equipment has 26 sensors, denoted as V1 to V26, which record values of different process variables such as electricity, liquid/gas flow rate, pressure, and so on. Figure 1 shows profiles of six selected sensors over 52 samples from six different product lots. First of all, it is clear to see that profile lengths vary from sample to sample, indicating the un-synchronization problem for different samples due to the self-controlled process.

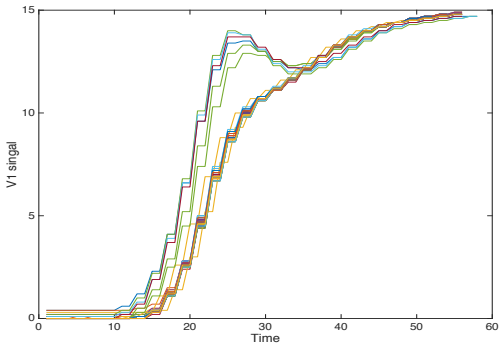

(a) V1

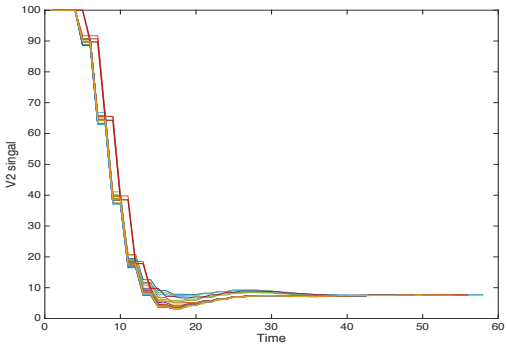

(b) V2

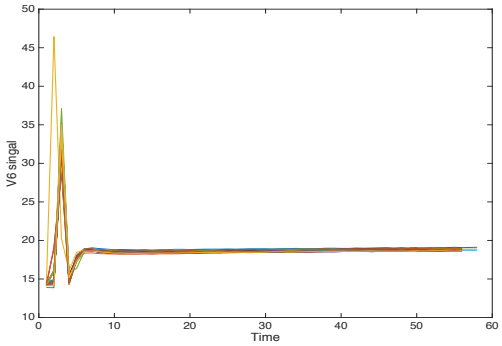

(c) V6

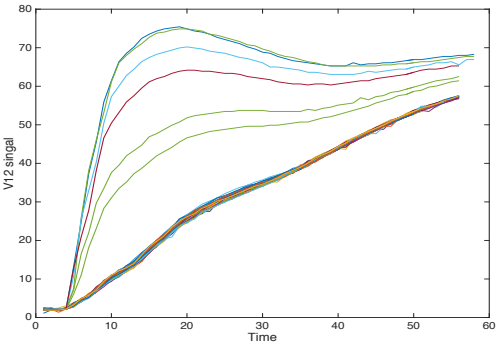

(d) V12

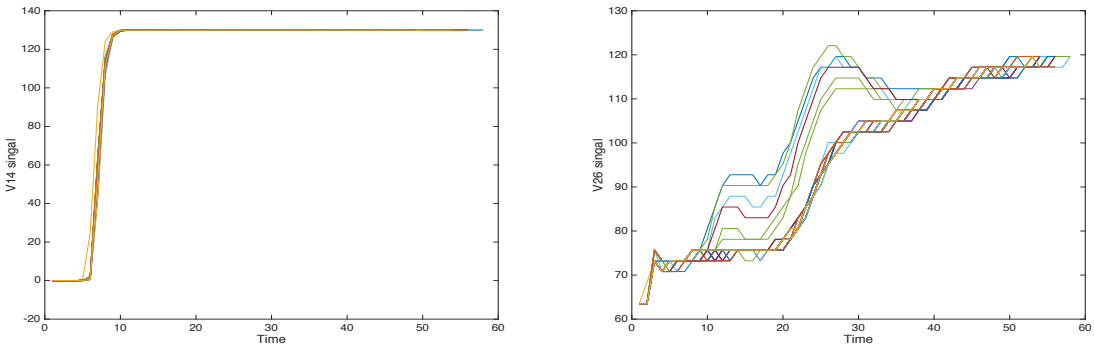

(e) V14 (f) V26

Figure 1. The six selected sensor profiles over 52 samples.

Second, all the profiles have smooth patterns over time, which show their strong within-profile correlations. To better demonstrate this point, we first do data alignment for different samples, and then calculate signal correlations of different time points (i.e., within-profile correlations) for every sensor. Figure 2 shows the within-profile correlation structure of V1, V6 and V14. In particular, all these sensors show strong within-profile correlations, and correlations of different sensors are quite different. This indicates that different sensors are driven by different system mechanisms and illustrate different features, which will be explained later in more details.

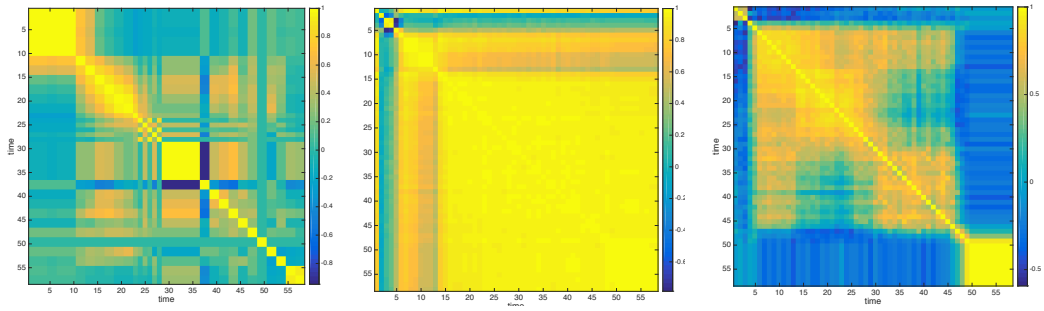

(a) V1 (b) V6 (c) V14

Figure 2. The within-profile correlations of V1, V6 and V14.

Third, besides within-profile correlations, different sensors have complex inter-profile relationships. As shown in Figure 1, for certain sensors, such as V1 and V26, their profiles share similar features. This is because these sensors measure some physically related process variables and are located near to each other. However, for some other sensors, such as V2 and V12, their profiles have quite different features. This is because that these sensors are located in different places or measure different process variables. The feature similarity can be evaluated by sensor cross-correlations to some degree. Sensors with similar features have strong cross-correlations, while sensors with different features have weak ones. Consequently, as the number of sensors increases, the chance that all sensors are strongly correlated is quite small, especially for high-dimensional cases. In other words, these multiple (multichannel) profiles can be naturally regarded as multi-mode data or mixture data. To make this point more explicit, for every sensor, we first synchronize profiles of all the samples to the same length using dynamic time warping (Keogh and Ratanamahatana (2005)). Then we take average of the synchronized profiles to get the template profile of every sensor. We subtract the sensor template profile from the synchronized profiles and get the corresponding residual profiles for every sensor. Finally, we use these residual profiles to calculate cross-correlations of these 26 sensors. From Figure 3, we can see that the cross-correlations have a blocky structure, based on which sensors can be naturally divided into several clusters with strong within-cluster cross-correlations. Furthermore, Figure 4 presents the residual profiles of V1. They have significant time-dependent variance. This is principally caused by fabrication "on-off" operations. They lead sensor signals to change drastically at some specific time points, where larger fluctuations are expected than other time points.

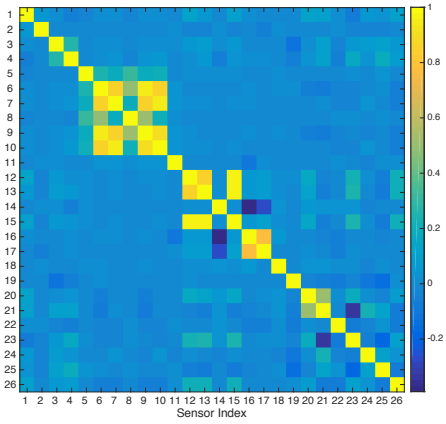

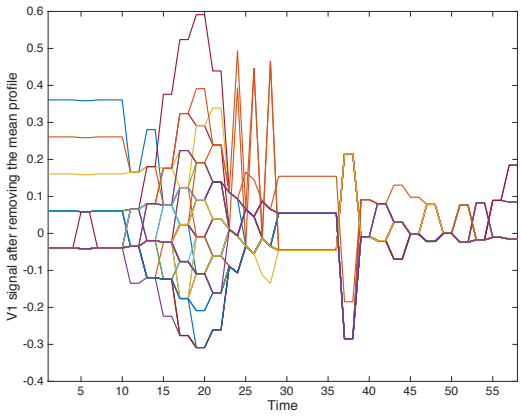

Figure 3. The cross-correlation structure of different sensors. Figure 4. The residual profiles of V1.

Finally, to demonstrate system inherent variations, Figure 5(a) shows profiles of V4 over the 52 samples, where sample colors have been arranged to change from light blue (first sample) to purple (last sample) according to the actual sample production start time. Obviously, there is a long-term drift that shifts the profiles downward from the beginning to the end of the production process. This drift may be caused by the change of equipment status due to the environmental disturbance over time, and hence should be regarded as normal operations to be taken into account in the monitoring scheme.

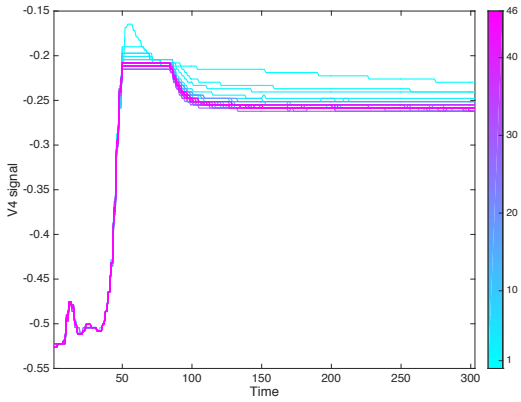

Figure 5. Long-term drift of V4.

1.2 Literature Review

In early work of profile data monitoring, Jin and Shi (1999, 2001) proposed to use wavelets to extract features of stamping tonnage signals for on-line fault detection. So far the topic of profile monitoring has received more and more attentions. The current literature can be generally classified into two major categories, i.e., linear and non-linear profile monitoring, according to profile shape complexities. For linear profiles, linear regression models are usually used to represent profile data, and regression coefficients are used for monitoring (Mahmoud and Woodall (2004), Zou et al. (2007)). However, these models assume *i.i.d* measurement noises within a profile. Later, to further effectively account for within-profile correlations, Jensen et al. (2008) proposed a linear mixed-effects model. For nonlinear profiles, nonparametric regression methods have been commonly used in profile monitoring, such as the spline regression (Walker and Wright (2002)), the wavelet regression (Zhou et al. (2006)), and the local linear smoothers (Zou et al. (2008)). Qiu et al. (2010) and Paynabar and Jin (2011) introduced nonlinear mixed-effects models considering within-profile correlations as well. Beyond these models, Ding et al. (2006) considered dimension reduction and data-clustering techniques for Phase I monitoring of nonlinear profiles. For more detailed discussions about related methods, please refer to Noorossana et al. (2011) and Woodall (2007) for a comprehensive review. However, the literature mentioned above only focuses on process with a univariate profile. Though for multichannel profiles, we may apply these methods for every channel separately, this completely ignores cross-correlations of multiple channels and weakens the detection power.

In the literature, few studies were conducted for monitoring multiple profiles simultaneously. For linear profiles with explanatory variables, Noorossana et al. (2010a, 2010b, 2016) and Ghashghaei and Amiri (2016) proposed several monitoring schemes based on the ordinary least square method. Zou et al. (2012) proposed a LASSO-based monitoring scheme. For nonlinear profiles, since signals are usually high-dimensional, dimension reduction methods are usually applied first to reduce data

dimensionality. For example, Kim et al. (2006) introduced a multichannel profile monitoring scheme using principal curves. Paynabar et al. (2013) proposed to use uncorrelated multi-linear principal component analysis (UMPCA) for feature extraction and fault detection. Later Grasso et al. (2014) compared multiple PCA-based methods, such as multi-linear PCA (MPCA) and vectorized PCA (or multi-way PCA, shortened as VPCA), for monitoring. Recently, Paynabar et al. (2015) further applied functional data analysis into profile monitoring, and constructed a change-point model based on multichannel functional PCA (MFPCA). However, all these aforementioned methods typically assume that multichannel profiles have strong cross-correlations with similar features, and cannot handle profiles with different features effectively. This is because that their extracted PCA loadings would mix different features together. Consequently, their monitoring performance will deteriorate severely (as demonstrated in our case study). So far to our best knowledge, no monitoring scheme is developed for profiles with different features from either statistical or practical perspective.

1.3 Our Contributions

Motivated by the previous work, the goal of this research is to design a systematic framework for on-line monitoring of high-dimensional streaming data in a manufacturing system. Our contributions are summarized as below: 1) We propose a preprocessing framework for manufacturing data considering their characteristics. In particular, for the product fabrication time variation problem, unless directly using naive interpolation methods (Lee et al. 2011), which brutally break profile patterns for different samples, we propose to use dynamic time warping to ensure the patterns are maximally preserved and the additional noise is minimally introduced. For long-term drift removing, we propose a fixed-effects model to learn drifting sensors, drifting time, and drifting magnitudes automatically. 2) After preprocessing, we propose a sensor clustering algorithm according to the sensor cross-correlation structure. Based on this algorithm, sensors within each cluster have strong correlations, while sensors

between clusters have no (or weak) correlations. In this way, we gather sensors with similar features together as a cluster and get several clusters with different features. 3) Since there is no more within-cluster feature difference, we can monitor sensor data within a cluster together and monitor each cluster respectively. In particular, MFPCA is applied for sensors of each separate cluster to extract their shared features. Then the MFPCA scores together with the residuals are used to construct local monitoring statistics to detect local changes in this cluster. 4) Finally, we proposed a data-fusion strategy to incorporate these local monitoring results together as the final monitoring statistic. Specifically, this statistic is based on the top-R rule, i.e., the sum of the largest R local monitoring statistics (Mei (2011)). This top-R rule can not only filter out IC noise and increase the detection sensitivity, but also allow for scalable detection power for different change patterns and assist the diagnostic procedure after an abnormal signal is triggered. The overview of the procedure is shown in Figure 6.

The remainder of this paper is organized as follows: Section 2 presents the data-preprocessing methods; Section 3 presents the monitoring scheme based on sensor clustering and data fusion; Section 4 evaluates the charting performance using some numerical studies in a manufacturing process; Finally, Section 5 concludes this paper with some discussions about the future work.

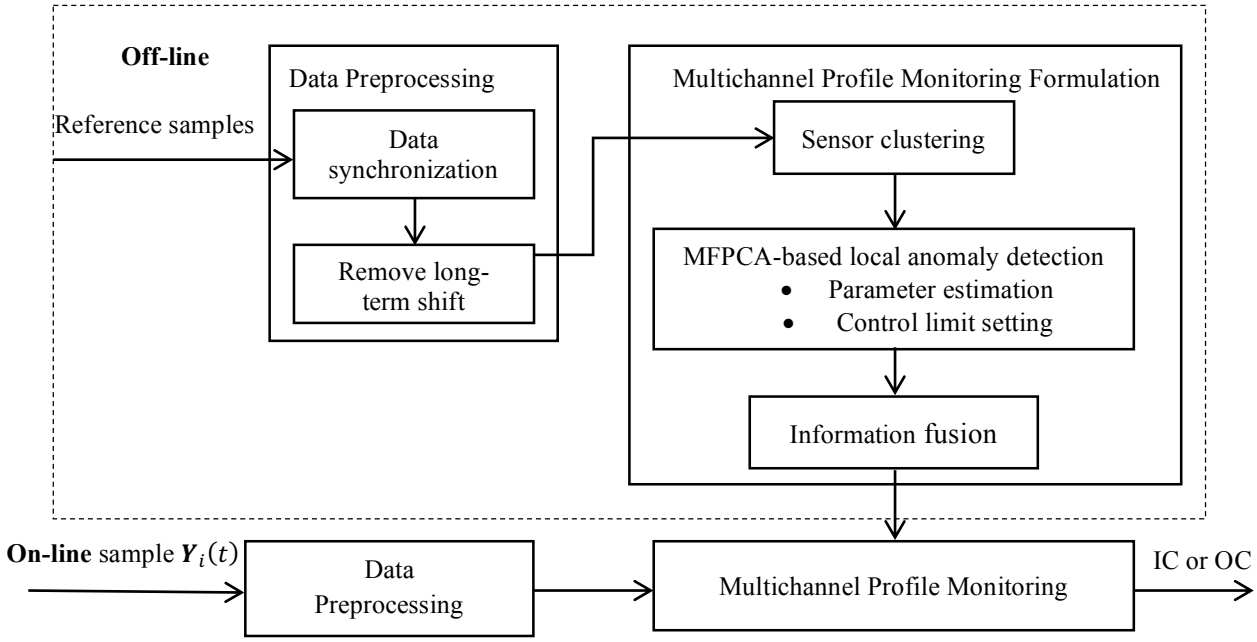

Figure 6. An overview of the developed monitoring system.

2. Data Preprocessing

In this section, we will discuss data preprocessing to address two issues: data alignments of multiple profiles, and long-term drift removal. Here we denote $i = 1, \dots, N;\ j = 1, \dots, P;$ and $t = 1, \dots, T_i$ for the indices of different samples, sensors, and time points, respectively. For example, Y_{ijt} indicates the scalar value of the j^{th} sensor at the t^{th} time point of the i^{th} sample. It should be noted that since the raw profiles of different samples may be unsynchronized, T_i are different for different samples.

2.1 Data Synchronization

As mentioned in Section 1, profile data has unsynchronized different lengths for different samples due to the self-controlled process in the manufacturing process. In this section, for every sensor j, we would like to synchronize the time stamp of the i^{th} sample by comparing its signals $Y_{ijt}, t = 1, \dots, T_i$, with the reference sample denoted by $Y_{1jt}, t = 1, \dots, T_1$ (here we set the first sample as the reference), using dynamic time warping (DTW) (Keogh and Ratanamahatana (2005)). To align these two

sequences using DTW, we first construct a T_1-by-T_i distance matrix where the (t_1, t_i) element corresponds to the square distance: $d(t_1, t_i) = \left(Y_{1jt_1} - Y_{ijt_i} \right)^2$. DTW aims to solve the optimal path $\left(t_1^l, t_i^l\right)_{l=1,\cdots,L}$ that minimizes the warping cost:

$$DTW\left(\boldsymbol{Y}_{1j}, \boldsymbol{Y}_{ij}\right) = \min\left\{\sum_{l=1}^{L} d\left(t_1^l, t_i^l\right)\right\},$$

where (t_1^l, t_i^l) is the index of the l^{th} element on the alignment path for the i^{th} sample.

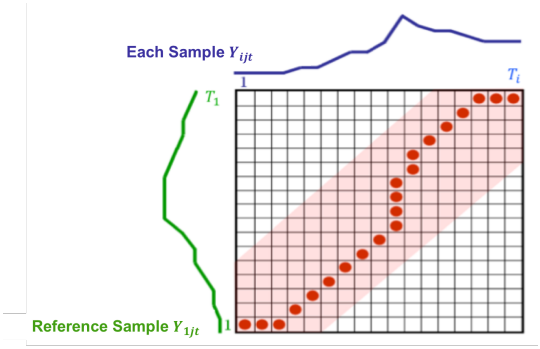

Figure 7. Dynamic time warping procedure.

Furthermore, we constrain the search space by the Sakoe-Chiba band constraint, i.e.

$$\left|t_1^l - t_i^l\right| \leq \max\left(0.2T_1, 0.2T_i, |T_1 - T_i|\right), l = 1, \cdots, L,$$

such that the optimal path is not too far from the diagonal line, as shown in Figure 7. The optimal path can then be found efficiently by dynamic programming. Finally, the optimal path provides a mapping from the i^{th} sample to the reference sample such that $(t_1^l, t_i^l)_{l=1,\ldots,L}$ is the optimal path that achieves the minimal warping cost. Therefore, profiles of each sample can be aligned to those of the reference sample. We show one example of how DTW can synchronize profiles of different samples in Figure 8.

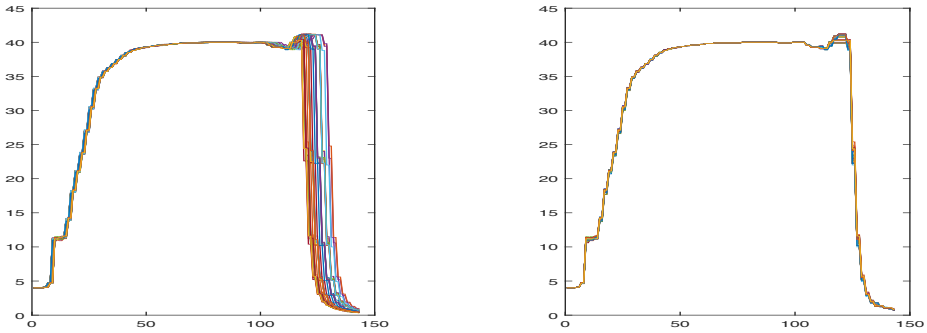

(a) Sample profiles before alignment (b) Sample profiles after alignment

Figure 8. Effect of alignment by DTW on V2.

2.2 Removing Long-term Drift

As shown in Figure 5(a), even for the same sensor, its long-term drift magnitude varies in different time segments. This phenomenon motivates us to estimate long-term drifts for different time segments separately. Generally, the long-term drift depends on the system status, which is influenced by the "on-off" operations. With this in mind, we may treat the time points between two sequential "on-off" operations as a nature segment. Specifically, after synchronization, all samples share the same time length T. These T time points can be separated into M steps, with Y_{ijt} given by

$$Y_{ijt} = \mu_{jt} + b_{ijm} + \epsilon_{ijt}, \qquad m = 1, \dots, M, \tag{1}$$

where m denotes the corresponding segment to which the t^{th} time point belongs. We define t_m as the last time point of the m^{th} segment, i.e., for the m^{th} segment of the profile, $t_{m-1} < t \leq t_m, m = 1, \dots, M$ with $t_0 = 0$. In Equation (1), μ_{jt} is the template signal of the j^{th} sensor at the t^{th} time point. b_{ijm} is assumed to be the constant drift of the j^{th} variable in the m^{th} time segment of the i^{th} sample, with respect to the template signals. ϵ_{ijt} denotes the remaining individual signal for $t = 1, \dots, T$, following a distribution with mean 0 and variance σ_{jt}^2. Following Lee et al. (2011), we apply the

weighted least squares (WLS) method to estimate parameters μ_{jt} and b_{ijm} by minimizing the weighted sum of squared errors (WSSE), i.e.,

$$\min_{\mu_{jt},b_{ijm}} WSSE_{jm} = \sum_{i=1}^{N} \sum_{t=t_{m-1}+1}^{t_m} \frac{1}{\sigma_{jt}^2} \left(Y_{ijt} - \mu_{jt} - b_{ijm}\right)^2, \quad \text{s.t.} \sum_{i=1}^{N} b_{ijm} = 0, \tag{2}$$

for $j = 1, \dots P, m = 1, \dots, M$, separately. Equation (2) can be solved in a close-form following the same approach in Lee et al. (2011). However, one limitation of this approach in Lee et al. (2011) is that the estimated $\hat{b}_{ijm}$ is not necessarily to be the long-term drift. Since it only denotes the constant difference of the i^{th} sample from the template profile in the m^{th} segment, caused by sample-to-sample variations. While for the true long-term drift, $\hat{b}_{ijm}$ should be a drift and expected to be monotone. In other words, the cumulative drift magnitude between neighbor samples, $\left|\sum_{i=2}^{N}(\hat{b}_{ijm} - \hat{b}_{(i-1)jm})\right| = \left|\hat{b}_{Njm} - \hat{b}_{1jm}\right|$, should be large enough when the true long-term drift exists. Therefore, we propose to apply hard thresholding to the estimated $\hat{b}_{ijm}$ as

$$\tilde{b}_{ijm} = \begin{cases} \hat{b}_{ijm}, & \text{if } \left|\hat{b}_{Njm} - \hat{b}_{1jm}\right| > s_{jm} \\ 0, & \text{otherwise} \end{cases}, \tag{3}$$

where s_{jm} is the threshold related to the variance of $\hat{b}_{ijm}$. In our study, we find that $s_{jm} = 3\times\text{std}\,(\hat{b}_{ijm})$ works very well in practice.

When σ_{jt}^2 is unknown, we can estimate it by $\hat{\sigma}_{jt}^2 = \sum_{i=1}^{N} \frac{\left(Y_{ijt} - \hat{\mu}_{jt} - \tilde{b}_{ijm}\right)^2}{N}$. Furthermore, it should be noted that when "on-off" operations do not change the profile too much, we may combine several sequential segments as one for analysis. From the data-driven perspective, we may redefine the

segments by setting $\{t_m|\hat{\sigma}^2_{jt_m} > s\}$, as segment boundaries, where s is a pre-specified threshold. In this paper, we set $s = 3\times\text{median}(\hat{\sigma}^2_{jt})$, and then iterate the above procedure to estimate $\hat{b}_{ijm}$, $\tilde{b}_{ijm}$, $\hat{\sigma}^2_{jt}$, and t_m. It is to be noted that M can change in different iteration steps. This estimation algorithm converges empirically in our numerical studies.

We demonstrate the efficiency of this algorithm using V2 as an example. Figure 9(a) shows the profiles of V2 in one processing step before removing the long-term drift, from which we can clearly see that these profiles have a long-term mean drift since $t = 50$. After iterating the algorithm until convergence, 4 segment boundaries satisfying $\{t_m|\hat{\sigma}^2_{jt_m} > s\}$ are identified as $t_1 = 50, t_2 = 51, t_3 = 52$ and $t_4 = 86$ (shown by the vertical dash lines in Figure 9(a)). However, only the last two segments [52,86] and [86,304] have nonzero $\tilde{b}_{ijm}$ to be removed, as shown in Figure 9(b). The final sample profiles after removing the drifts $\tilde{b}_{ijm}$ are shown in Figure 9(c).

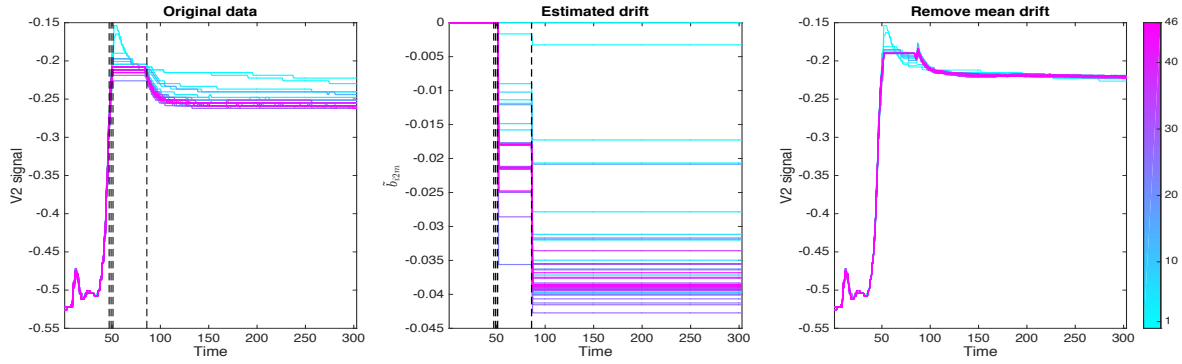

(a) Original profiles (b) Estimated drift (c) Profiles after removing the drift

Figure 9. Remove the long-term drift of V2.

3. Multichannel Profile Monitoring Formulation

In this section, we will introduce the multichannel profile monitoring scheme in detail. We treat a profile as a function and adopt functional data analysis (FDA) for data description and monitoring. In

particular, we consider the aligned profile data of the i^{th} sample of the j^{th} sensor as a continuous function $Y_{ij}(t)$ with respect to $t \in \mathcal{T} = [a, b]$, where $[a, b]$ is the manufacturing time interval. The observations $Y_{ijt}, t = 1, \dots, T$, are discrete sensing observations of the function at T sampling time points $t = 1, \dots, T$. According to Equation (1), after removing the long-term drift, $Y_{ij}(t)$ can be formulated as

$$Y_{ij}(t) = \mu_j(t) + \epsilon_{ij}(t), \qquad i = 1, \dots N;\ j = 1, \dots, P, \tag{4}$$

where $\mu_j(t)$ is the function of the template profile of the j^{th} sensor solved in Equation (2), and $\epsilon_{ij}(t)$ is the stochastic error with $E\left(\epsilon_{ij}(t)\right) = 0$. Then profile data of all the sensors can be denoted as $\boldsymbol{Y}_i(t) = [Y_{i1}(t), \dots, Y_{iP}(t)]$, with $\boldsymbol{\mu}(t) = [\mu_1(t), \dots, \mu_P(t)]$, and $\boldsymbol{\epsilon}_i(t) = [\epsilon_{i1}(t), \dots, \epsilon_{iP}(t)]$. Our goal is to sequentially monitor distributional changes of $\boldsymbol{\mu}(t)$.

Assume that there are m_0 *i.i.d* reference samples $\boldsymbol{Y}_{-m_0+1}(t), \dots, \boldsymbol{Y}_0(t)$ (or IC samples interchangeably), when the process is in control. Then in the sequential monitoring stage, the subsequent i^{th} on-line testing sample after preprocessing, i.e., $\boldsymbol{Y}_i(t)$, assumes following a change-point model

$$\boldsymbol{Y}_i(t) = \begin{cases} \boldsymbol{\mu}_0(t) + \boldsymbol{\epsilon}_i(t), & \text{for } i = 1, \dots, \tau, \\ \boldsymbol{\mu}_1(t) + \boldsymbol{\epsilon}_i(t), & \text{for } i = \tau + 1, \dots \end{cases} \tag{5}$$

where τ is the unknown change point, $\boldsymbol{\mu}_0(t)$ and $\boldsymbol{\mu}_1(t)$ are the IC and OC mean (template) functions. We aim to detect the OC situation as soon as possible and estimate the change point τ as accurate as possible.

As discussed earlier, sensor profiles from the same source have similar features and are cross-correlated. Thus, it is intuitive to consider their correlation structure and use multivariate SPC

schemes for joint monitoring. However, sensor profiles from different sources have different features and can be regarded as different clusters. Therefore, it is not effective to construct a universal monitoring scheme without considering feature difference. Furthermore, due to the sparsity of OC variables, jointly monitoring all sensors without selecting correlated clusters may dilute detection power. As Figure 3 shows, the 26 sensors are sparsely correlated with a clusterwise correlation structure. This clusterwise structure naturally motivates us the idea of "divide and conquer". With these in mind, we propose a monitoring scheme based on sensor clustering and fusion. Its key idea is to first partition multiple sensors into several sensor clusters so that sensors in the same cluster share similar features, and feature difference only exists in different clusters. Then we construct local monitoring statistics for each sensor cluster separately by taking advantage of the local correlation structure. Finally, these local monitoring statistics are fused together by summing up the largest R local test statistics for final decision making. In this way, the united monitoring scheme can on the one hand take into account both feature similarity and feature difference. On the other hand, it can filter out IC noise, without scarifying detection power too much, and therefore improve detection power for sparse changes. Furthermore, it is convenient for us to identify the set of potentially changed sensors, by selecting sensors whose groups are included in the largest R local test statistics. This "divide and conquer" idea has been successfully used in some other SPC schemes (Zhang et al. 2016).

3.1 Sensor Clustering

In this subsection, we will discuss how to cluster multichannel profiles based on m_0 reference samples $\boldsymbol{Y}_{-m_0+1}(t), \ldots, \boldsymbol{Y}_0(t)$. As mentioned in Section 1.1, sensor profiles can be naturally clustered according to their cross-correlation matrix. Therefore, here we adopt the agglomerative hierarchical correlation clustering method, which begins with treating each sensor as a separate cluster and then successively merges them into larger clusters according to sensor correlations. In each step of hierarchical clustering, the algorithm finds the closest pair of clusters and then merges them into a

new parent cluster. It is repeated until only one cluster is left after $P-1$ iterations where P is the number of sensors. Here the Pearson's correlation is used to measure the similarity between different sensors, which can be estimated as

$$\rho_{jj'} = \frac{\sum_{i=-m_0+1}^{0}\sum_{t=1}^{T}(Y_{ijt}-\bar{Y}_{jt})(Y_{ij't}-\bar{Y}_{j't})}{\sqrt{\sum_{i=-m_0+1}^{0}\sum_{t=1}^{T}(Y_{ijt}-\bar{Y}_{jt})^2}\sqrt{\sum_{i=-m_0+1}^{0}\sum_{t=1}^{T}\left(Y_{ij't}-\bar{Y}_{j't}\right)^2}}, \quad (6)$$

for $j, j' = 1, \dots, P$, where $\bar{Y}_{jt} = \frac{1}{m_0}\sum_{i=-m_0+1}^{0} Y_{ijt}$. Then the distance (dissimilarity) between different sensors is defined as

$$d_{jj'} = 1 - |\rho_{jj'}|, \qquad j, j' = 1, \dots, P. \quad (7)$$

We can see that the more correlated the two sensors are, the shorter their distance will be. In addition to the distance between two sensors, cophenetic distance with the average linkage, i.e., $D(r,k) = \frac{\sum_{v\in r}^{N_r}\sum_{u\in k}^{N_k} d_{vu}}{N_r N_k}$, is used to measure the between-cluster distance of clusters r and k, where N_r and N_k are the number of sensors in clusters r and k. Then in every step, according to $D(r,k)$, we can select two most similar clusters and merge them into one. This sequential merging procedure can be drawn as a dendrogram, based on which, we can finally get the sensor information of every cluster, given a pre-specified number of clusters, G.

The optimal choice of *G* will balance the model accuracy and complexity. In general, a small *G* leads to larger clusters, less estimation accuracy, and low complexity, and *vice versa*. In real applications, the choice of *G* can depend on some prior domain knowledge. For example, in our case study, the optimal *G=16* is selected based on the domain knowledge that the minimum correlation between two sensors in the same cluster is no smaller than 0.2. In general, when no *G* is preferred in advance, some

clustering diagnostic methods, such as the elbow method of Thorndike, R.L. (1953), the GAP statistic of Tibshirani et al. (2001), could be used to choose G.

3.2 Multichannel Functional PCA – based Local Anomaly Detection

Assume after sensor clustering, we have G clusters in total with each cluster having p^g sensors where $g = 1, \dots, G$. Then the profile data for each cluster can be denoted as $\boldsymbol{Y}_i^g(t) = \left[Y_{i1}(t), \dots, Y_{ip^g}(t)\right]$, with the corresponding template profile $\boldsymbol{\mu}^g(t) = \left[\mu_1(t), \dots, \mu_{p^g}(t)\right]$ and stochastic error $\boldsymbol{\epsilon}_i^g(t) = \left[\epsilon_{i1}(t), \dots, \epsilon_{ip^g}(t)\right], i = 1, \dots, N$. Then we will discuss how to construct local monitoring statistics for $\boldsymbol{Y}_i^g(t)$, to detect changes of $\boldsymbol{\mu}^g(t), g = 1, \dots, G$, separately. In the next subsection, we will address how to fuse the G local statistics together as the final monitoring statistic to detect changes of $\boldsymbol{\mu}(t)$.

A straightforward monitoring statistic for $\boldsymbol{Y}_i^g(t)$ is to apply the traditional parametric or nonparametric SPC methods. However, in many situations, the total number of grid time points, i.e., $T \times p^g$, is much larger than the number of IC reference samples, m_0. Then we will suffer the curse of dimensionality. Hence it is usually important to perform dimension reduction before the monitoring step. One fundamental technique is to use functional PCA (FPCA) to extract a few major and typical features from the functional data. FPCA has been applied in univariate Phase I profile monitoring in Yu et al. (2012). Recently, Paynabar et al. (2015) extended FPCA to multichannel profiles as MFPCA, by appropriately addressing their cross-correlations.

In particular, Paynabar et al. (2015) assumes that $\boldsymbol{Y}_i^g(t)$ can be represented by a set of orthonormal eigenfunctions as follows,

$$\boldsymbol{Y}_i^{\boldsymbol{g}}(t) = \boldsymbol{\mu}_0^{\boldsymbol{g}}(t) + \sum_{k=1}^{\infty} \boldsymbol{\xi}_{ik}^g \, v_k^g(t), \tag{8}$$

with an explicit form $\boldsymbol{\xi}_{ik}^{g} = \int_a^b (\boldsymbol{Y}_i^g(t) - \boldsymbol{\mu}_0^g(t)) v_k^g(t) dt$, where $v_k^g(\cdot), k = 1,2, \ldots \infty$, are the eigenfunctions of the covariance function of $\boldsymbol{Y}_i^g(t)$, i.e., $c^g(t,s) = E\left[(\boldsymbol{Y}^g(t) - \boldsymbol{\mu}_0^{\boldsymbol{g}}(t))(\boldsymbol{Y}^g(s) - \boldsymbol{\mu}_0^{\boldsymbol{g}}(s))\right]$, with the corresponding eigenvalues $\lambda_k^g, k = 1,2, \ldots \infty$. In particular, $c^g(t,s)$ can be estimated using the m_0 reference samples as

$$\hat{c}^g(t, s) = \frac{1}{m_0} \sum_{i=-m_0+1}^{0} \sum_{j=1}^{p^g} (Y_{ij}^g(t) - \mu_{0j}^g(t))(Y_{ij}^g(s) - \mu_{0j}^g(s)). \quad (9)$$

When $\mu_{0j}^g(t)$ is unknown in practice, we substitute it by its estimate $\hat{\mu}_{0j}^g(t) = \sum_{i=-m_0+1}^{0} Y_{ij}^g(t) / m_0$ using the historical reference data. Then the corresponding estimators of $v_k^g(\cdot)$ and λ_k^g are defined as

$$\int_a^b \hat{c}^g(t,s)\, \hat{v}_k^g(s) ds = \hat{\lambda}_k^g \hat{v}_k^g(t), \quad t \in \mathcal{T}, \; k = 1,2, \ldots, \infty. \quad (10)$$

Under some mild conditions, $\hat{c}^g(t,s)$, $\hat{v}_k^g(t)$ and $\hat{\lambda}_k^g$ are consistent estimators of $c^g(t,s), v_k^g(t)$ and λ_k^g (Paynabar et al. (2015)).

The form of Equation (8) indicates that all the p^g profiles share a common set of eigenfunctions, and their cross-correlations are essentially described by the correlations of $\boldsymbol{\xi}_{ik}^g$. In particular, we assume $\boldsymbol{\xi}_{ik}^g \in \mathbb{R}^{p^g}$ follows a p^g-dimensional normal distribution with mean $\mathbf{0}$ and covariance matrix $\boldsymbol{\Sigma}_k^g$, which can be estimated using the m_0 reference samples as

$$\widehat{\boldsymbol{\Sigma}}_k^g = \frac{1}{m_0} \sum_{i=-m_0+1}^{0} \int_a^b (\boldsymbol{Y}_i^g(t) - \boldsymbol{\mu}_0^g(t)) \hat{v}_k^g(t) dt \int_a^b \left(\boldsymbol{Y}_i^g(t) - \boldsymbol{\mu}_0^g(t)\right)^T \hat{v}_k^g(t) dt. \quad (11)$$

Furthermore, since $\hat{\boldsymbol{\xi}}_{ik}^g$ is the projection of $(\boldsymbol{Y}_i^{\boldsymbol{g}}(t) - \boldsymbol{\mu}_0^g(t))$ to the k^{th} eigenfunction, it is an ideal indicator that reflects the difference between the i^{th} sample $\boldsymbol{Y}_i^g(t)$ and $\boldsymbol{\mu}_0^g(t)$. In particular, $\hat{\boldsymbol{\xi}}_{ik}^g$ shows the amount of deviation of the i^{th} sample from the k^{th} variation mode. If $\boldsymbol{Y}_i^g(t)$ is out of control,

$\hat{\boldsymbol{\xi}}_{ik}^{\boldsymbol{g}} \rightarrow^{d} N\left(\int_a^b \left(\boldsymbol{\mu}_1^g(t) - \boldsymbol{\mu}_0^g(t)\right) \hat{v}_k^g(t)dt\,, \boldsymbol{\Sigma}_k^g\right)$ (Paynabar et al. (2015)). In this way, we can construct a hypothesis test using $\hat{\boldsymbol{\xi}}_{ik}^{\boldsymbol{g}}$. Here we chose the largest $\hat{\boldsymbol{\xi}}_{ik}^{g}, k = 1, \ldots, d$, for monitoring. To further improve the detection performance on small mean shifts, we adopt the exponential weighted moving average (EWMA) strategy and define

$$\boldsymbol{X}_i^g(t) = (1-w)\boldsymbol{X}_{i-1}^g(t) + w\boldsymbol{Y}_i^g(t), \tag{12}$$

$$\boldsymbol{z}_{ik}^g = \int_a^b (\boldsymbol{X}_i^g(t) - \boldsymbol{\mu}_0^g(t))\, \hat{v}_k^g\,(t)dt, k = 1, \ldots, d, \tag{13}$$

where $\boldsymbol{X}_0^g(t)$=**0** and w is the exponential weighting parameter**.** In practice, the common choice of w is in the interval [0.05,0.2]. Thus, the final test statistic for the i^{th} on-line sample is defined as

$$Z_i^g = \sum_{k=1}^d \boldsymbol{z}_{ik}^{gT} \left(\hat{\boldsymbol{\Sigma}}_k^g\right)^{-1} \boldsymbol{z}_{ik}^g. \tag{14}$$

It should be noted that Z_i^g can only detect changes that are captured by $\hat{v}_k^g\,(t), k = 1, \ldots, d$. For changes that are captured by higher order projections, $\hat{v}_k^g\,(t), k = d+1, \ldots,$ similar to the residual chart of traditional PCA-based monitoring schemes (Jackson and Mudholkar (1979)), we propose a corresponding residual chart for Z_i^g. Specifically, we calculate the residual of the approximation of $\boldsymbol{Y}_{\boldsymbol{i}}^{\boldsymbol{g}}(t)$ using the first d eigenfunctions

$$\boldsymbol{e}_i^g(t) = \boldsymbol{Y}_i^g(t) - \sum_{k=1}^d \hat{\boldsymbol{\xi}}_{ik}^g \hat{v}_k^g\,(t), \tag{15}$$

and its EWMA form as

$$\boldsymbol{r}_i^g(t) = (1-w)\boldsymbol{r}_{i-1}^g(t) + w\boldsymbol{e}_i^g(t), \tag{16}$$

with $\boldsymbol{r}_0^g(t)$=**0**. Then we construct the residual chart for the i^{th} sample using the square of the norm of $\boldsymbol{r}_i^g(t)$ as

$$Q_i^g = \sum_{j=1}^{p^g} ||\boldsymbol{r}_{ij}^g||^2 = \sum_{j=1}^{p^g} \int_a^b \{r_{ij}^g(t)\}^2 dt. \quad (17)$$

For a cluster with a single sensor, i.e., $p^g = 1$, MFPCA degenerates to the traditional FPCA. Then the procedure above (Equation (8)-(17)) is a Phase II control chart for univariate profile based on FPCA, which is the counterpart of the Phase I control chart of Yu et al. (2012).

3.3 Information Fusion via Top-*R* Thresholding Rule

Suppose that we have divided all the *P* sensors into *G* clusters and calculated $\{Z_i^g, Q_i^g\}, g = 1, \ldots, G$. The next problem is how to combine these local monitoring statistics of each cluster to produce a global monitoring statistic to detect OC conditions as quickly as possible, subject to a pre-specified system-wise false alarm rate. An intuitive way to construct the global monitoring statistic is to sum all local monitoring statistics together (Mei (2010)). However, though this global monitoring statistic usually performs well for small mean shifts among all the sensors, it is not suitable for the case of mean shifts that only occur in a few sensors, due to the additional noise introduced by the local monitoring statistics for unchanged sensors. As a complementary therapy, the maximum chart (Tartakovsky et al. (2006)) aims to detect large but sparse shifts by only selecting the largest local monitoring statistic. However, this selection clearly renders its poor performance if more than one sensor changes. Mei (2011) and Liu et al. (2015) proposed a top-*R* rule to balance between the sum and the maximum chart by summing the largest *R* local monitoring statistics as the global monitoring statistic. Furthermore, this top-*R* rule is particularly effective when we have some prior domain knowledge that at most *R* out of *G* data streams will be affected by an abnormal event. Motivated by this, we propose to fuse the *G* local monitoring statistics with the top-*R* rule. However, since p^g are

different for different clusters, we need to normalize these local monitoring statistics firstly as $\{\tilde{Z}_i^g, \tilde{Q}_i^g\}, g = 1, \ldots, G$, to make them share the same mean 0 and standard deviation 1, i.e.,

$$\tilde{Z}_i^g = \frac{Z_i^g - E(Z_i^g)}{std(Z_i^g)}, \qquad \tilde{Q}_i^g = \frac{Q_i^g - E(Q_i^g)}{std(Q_i^g)}. \tag{18}$$

Then we rank the test statistics $\tilde{Z}_i^{(1)} \geq \cdots \geq \tilde{Z}_i^{(G)}$, $\tilde{Q}_i^{(1)} \geq \cdots \geq \tilde{Q}_i^{(G)}$ and propose to fuse these monitoring statistics as

$$T_i = \sum_{r=1}^{R} \tilde{Z}_i^{(r)}, \quad W_i = \sum_{r=1}^{R} \tilde{Q}_i^{(r)}. \tag{19}$$

Then if $T_i > h_T \; or \; W_i > h_W$, the monitoring scheme triggers an OC alarm for the i^{th} sample. Here h_T and h_W are the control limits according to the pre-specified system-wise IC average run length (ARL_0). In particular, we set h_T and h_W by simulation to ensure that the separate T chart and W chart have the same *IC ARL*, which is almost equal to $2\times ARL_0$, and in the meantime the joint T and W chart has the *IC ARL* equal to ARL_0.

In general, the choice of *R* depends on the specific OC scenario of most interest. As mentioned in Mei (2011) and Liu et al. (2015), a larger *R* leads to a better detection performance for global anomaly patterns which may occur in a lot of sensors yet with small magnitudes, while a smaller *R* results in a better detection performance for extreme anomaly patterns which only occur in few sensors yet with large magnitudes.

4. Case Study

In this section, we revisit the manufacturing process in Section 1 and use it as a case study to illustrate the proposed monitoring framework. As mentioned earlier, $P = 26$ sensors of different types, denoted as V1 to V26, are used to monitor the process. In the dataset, we have 46 IC samples. We first applied

DTW to remove the non-synchronization effect for different samples. After this, all the samples have the time length $T = 58$. Then we remove the long-term drift using the data-driven approach proposed in Section 2.2.

To construct the monitoring scheme, the first step is to cluster the sensors. Figure 10 shows the hierarchical clustering dendrogram of the 26 sensors with the y axis as the cophenetic distance between different clusters. Based on the dendrogram, we divide the 26 sensors into several clusters to ensure that the minimum correlation between two sensors in the same cluster is larger than 0.2. Finally, 16 clusters are achieved as

$$\{23, (20,21), 25, (3,4), 24,19, (6,7,9,10), (5,8), 1,26,22,2,18,11, (14,16,17), (12,13,15)\},$$

where sensors inside each pair of parentheses belong to the same cluster and sensors without parentheses are individual clusters. By reordering the sensors, the strong within-cluster correlations and weak between-cluster correlations are clearly shown in Figure 11. We also consider two other extreme scenarios with $G = 1$ or $G = 26$ for mere comparison, but for no recommendation. In particular, the chart with $G = 1$ treats all sensors as one cluster, which is the exact monitoring scheme based on MFPCA (extension of Paynabar et al. (2016) to Phase II). The chart with $G = 26$ treats every single sensor as a cluster, which is the monitoring scheme based on FPCA for every sensor separately (extension of Yu et al. (2012) to Phase II). As to the number of R in the monitoring scheme, according to the engineering domain knowledge, we know that the maximum number of changed sensors is not larger than 10. Therefore, we set $R = \{1,2,3,6,8,10,26\}$ separately for $G = 26$, $R = \{1,2,3,6,16\}$ separately for $G = 16$, and $R = 1$ for $G = 1$. In particular, $R = 1$ corresponds to the maximum chart, and $R = G$ corresponds to the sum chart. Furthermore, we also compare our clustering based monitoring schemes with three other state-of-the-art methods for multichannel profile monitoring, including the uncorrelated multilinear PCA (UMPCA) based monitoring scheme

(Paynabar et al. 2013), the multilinear PCA (MPCA) based monitoring scheme (Grasso et al. 2014), and the vectorized PCA (VPCA) based monitoring scheme (Nomikos and MacGregor 1995).

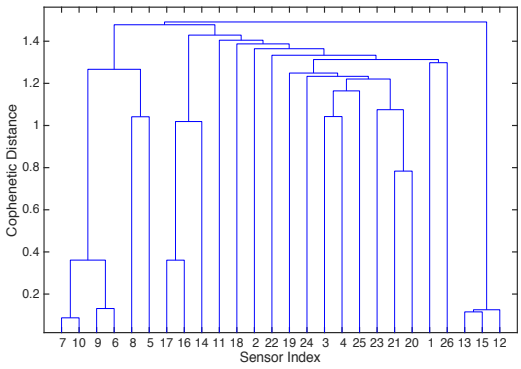

Figure 10. Hierarchical Clustering for sensors.

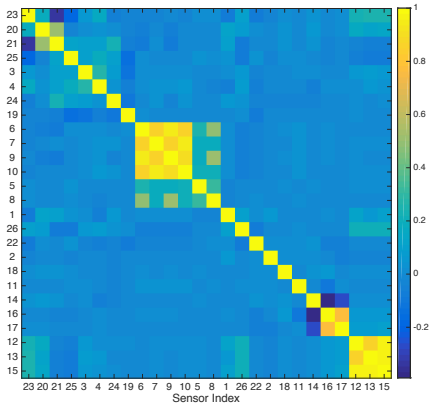

Figure 11. The correlation structure of re-ordered sensors based on the clustering result.

To evaluate the chart performance, we generate some OC patterns with different shift magnitudes purposely from the IC samples as OC samples for testing. These generated OC patterns mimic the true anomaly patterns in the manufacturing process. Specifically, we consider the following four types of OC shift patterns.

- **Mean shift** in sensor $j \in \{5,6,7,8,9,10,16,17\}$ of magnitude $\delta \times \left(\sum_{t=1}^{T} \hat{\sigma}_{jt} / T\right)$ in the entire time duration, i.e., $\mu_{1,j}(t) = \mu_{0,j}(t) + \delta \times (\sum_{t=1}^{T} \hat{\sigma}_{jt}/T)$ for $t \in (0,58]$, where $\hat{\sigma}_{jt}$ is the estimated standard division of the j^{th} sensor at t.
- **Slope shift** in sensor $j \in \{14,16,17\}$ of magnitude $\delta \times s_j(t)$ in the entire time duration, i.e., $\mu_{1,j}(t) = \mu_{0,j}(t) + \delta \times s_j(t)$ for $t \in (0,58]$, where $s_j(t)$ is a pre-specified slope change pattern for the j^{th} sensor at the time point t. Here we determine $s_j(t)$ from real OC samples in the process.
- **Spike shift** in sensor $j \in \{2,14,16,17\}$ at the time point $t = 51$ of magnitude $\delta \times (\sum_{i=1}^{46} ||\boldsymbol{Y}_{ij}||^2 / 46)$, i.e., $\mu_{1,j}(51) = \mu_{0,j}(51) + \delta \times (\sum_{i=1}^{46} ||\boldsymbol{Y}_{ij}||^2 / 46)$, where $||\boldsymbol{Y}_{ij}||^2$ is the square of the l_2 norm of the j^{th} sensor in the whole time duration for the i^{th} IC sample.

- **Joint shift** in sensor $j \in \{5,6,7,8,9,10,16,17\}$: fluctuation in sensor $j \in \{5,7,9,16,17\}$ in the time interval $t \in [20,58]$ of magnitude δ, i.e., $\mu_{1,ij}(t) = \mu_{0,ij}(t) + s_{ij}(t)$, where $s_{ij}(t) \sim N(0, \delta \times (\sum_{t=20}^{58} \hat{\sigma}_{jt}/39))$; constant mean shift in sensor $j \in \{6,8,10\}$ in the time interval $t \in [20,58]$ of magnitude $\delta \times (\sum_{t=20}^{58} \hat{\sigma}_{jt}/39)$, i.e., $\mu_{1,j}(t) = \mu_{0,j}(t) + \delta \times (\sum_{t=20}^{58} \hat{\sigma}_{jt}/39)$.

Illustrations of these generated OC patterns are shown in Figure 12 (It should be noted that the shift sizes δ in the figure are magnified more than those in the simulation, for simple illustration purpose). We consider two EWMA parameters, $w = 0.1$ and $w = 0.05$, separately. For each w, we tune the corresponding control limits, h_T and h_Q, for every chart to make its $ARL_0 = 200$. Then we evaluate the OC performance of different charts by simulation. In particular, in every simulation replication, we randomly draw $m_0 = 100$ IC samples with replacement as reference samples from the 46 IC samples, then we draw the subsequent samples from the generated OC samples sequentially as on-line testing samples. The monitoring scheme runs until an OC alarm is generated, and the corresponding run length of this replication is recorded. This procedure is replicated 2,000 times, and the estimated *OC ARL* and the standard deviation of run length (*SDRL*) for different charts are reported in Table 1 and Table 2 for $w = 0.1$, and Table 3 and Table 4 for $w = 0.05$.

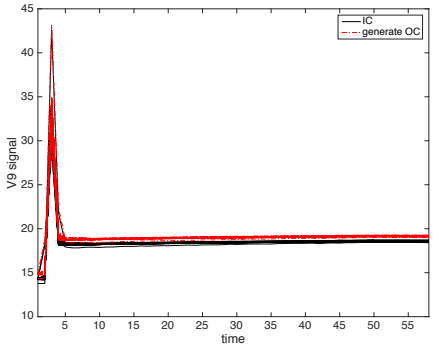

(a) Mean shift of V9 with $\delta = 5$

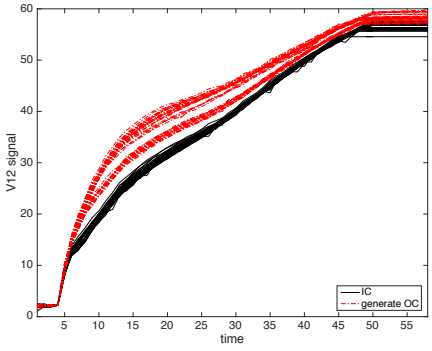

(b) Slope shift of V12 with $\delta = 0.2$

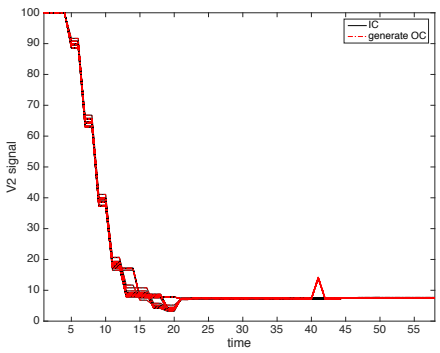

(c) Spike shift of V2 with $\delta = 0.2$

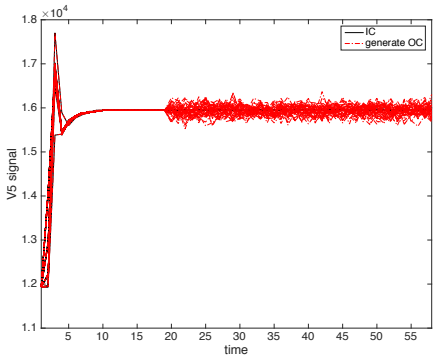

(d) Joint shift: fluctuation of V5 with $\delta = 5$

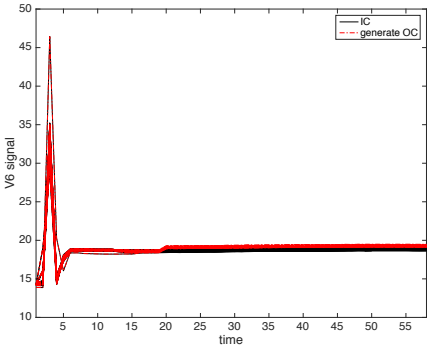

(e) Joint shift: mean shift of V6 with $\delta = 5$

Figure 12. Illustration of the generated OC patterns.

We can see that in general, the charts with $G = 16$ perform the best for detecting these four change patterns, followed by those with $G = 26$, while the charts with $G = 1$ have the poorest results. As stated previously, this is because that the charts with $G = 1$ fail to capture features of different sensor clusters since they assume all sensors come from the same cluster. On the contrary, by treating every profile separately, the charts with $G = 26$, though successfully capture different features from each sensor, are unable to capture sensor cross-correlations. Finally, we observe that the proposed charts with $G = 16$ can make a tradeoff between $G = 1$ and $G = 26$ and achieve the best results. Furthermore, among the charts with $G = 16$, those with R close to the number of clusters that include the changed sensors give the best results, such as $R = 3$ for the mean shifts and the joint shifts, $R = 1$

for the slope shifts, and $R = 2$ for the spike shifts. This is because that the charts with a smaller R (such as the maximum chart as the extreme case) fail to select all the changed sensor(s). However, the charts with a larger R (such as the sum chart) may dilute the detection power by involving too many unchanged sensors. This phenomenon also occurs in the charts with $G = 1$ or $G = 26$. In practice, we may adjust R according to the domain knowledge, to achieve the optimal detection power, which demonstrates the flexibility and efficiency of the top-R rule. As to the other three charts without considering sensor feature difference, i.e., MPCA, VPCA, and UMPCA, they perform very unsatisfactorily. In particular, for the slope shift and joint shift, all of these three charts loss their detection power. For the other two shifts, though MPCA performs comparably better than the other two charts, its detection power is still much worse than our proposed method. Furthermore, UMPCA generally has the worst performance among all the charts. This is due to its inherent limitation that the maximum number of PCs that can be extracted is no more than $\min\{g^k, m_0, T\}$. As a result, the explained data variation by UMPCA is very limited, rendering its poor performance for modeling and detection.

Furthermore, all the charts with $w = 0.05$ have better detection power for smaller shifts, while all the charts with $w = 0.1$ perform better for larger shifts. This is consistent with performance of general EWMA-type charts. In practice, the selection of w mainly depends on the expected true mean shift that we would like to detect.

5. Concluding Remarks

Though anomaly detection in manufacturing has been studied extensively in the literature, the following three challenges associated with efficient real-time monitoring for manufacturing process variables are yet to be addressed due to large system variation, complex sensor correlation structure, different sensor features, and sparse OC change patterns. This paper presents a monitoring framework, to fill in this gap. Specifically, we first propose data preprocessing methods to remove system inherent

variations, including the product fabrication time un-synchronization and manufacturing equipment long-term drift. Then to deal with sensor feature difference, we divide the sensors into several clusters according to their correlation structure. In this way, sensors in the same cluster share common features and sensors in different clusters have different features. Then for each cluster, we use MFPCA to extract the common features and construct local monitoring statistics based on the MFPCA scores and residuals, to detect local changes in each cluster. Collectively, with the top-R rule, these local monitoring statistics are fused together as a global monitoring statistic, which can have efficient and scalable detection power for sparse OC patterns. Finally, a case study with real data from a manufacturing process demonstrates the efficacy of the proposed framework in terms of OC ARL.

Along with this direction, there are still several valuable extensions. First, the current hierarchical clustering algorithm treats every time point of a profile as an independent observation without considering within-profile correlations. It is desirable to construct a more advanced clustering algorithm taking within-profile correlations into account. Second, the current monitoring framework considers two separate steps, sensor clustering, and data fusion, to deal with different sensor features. However, it might not be so straightforward or distinguishable to identify different clusters in some cases. With this regard, it is of interest to construct a uniform monitoring scheme that can handle different sensor features directly. Last but not the least, diagnostics is equally important as change detection. As such, we may consider developing a diagnostic procedure for the current monitoring scheme, after an OC alarm is triggered.

6. Acknowledgment

The authors are grateful for the valuable comments provided by the editors and referees. This paper is partially supported by the NSF grant ID: 1233143.

Table 1. *OC **ARL*** and *SDRL* in detecting slope shifts and mean shifts when $m_0 = 100$ and $w = 0.1$.

		G=26 (FPCA)							G=16					G=1 (MFPCA)	Other methods		
	δ	R=1	R=2	R=3	R=6	R=8	R=10	R=26	R=1	R=2	R=3	R=6	R=16	R=1	MPCA	VPCA	UMPCA
IC	0	**204**	**197**	**200**	**206**	**204**	**207**	**193**	**197**	**193**	**197**	**199**	**196**	**193**	**200**	**197**	**200**
		165	159	161	158	157	157	151	162	159	159	157	150	158	197	178	177
slope	0.01	**32.8**	**18.2**	**19.8**	**31.1**	**34.9**	**29.6**	**41.2**	**24.7**	**52.1**	**89.9**	**91.0**	**97.0**	**194**	**222**	**188**	**187**
		29.1	*10.2*	*11.5*	*23.9*	*29.1*	*20.7*	*30.9*	*58.0*	*60.9*	*103.8*	*25.1*	*28.4*	*155*	*201*	*176*	*171*
	0.02	**5.14**	**4.55**	**4.36**	**4.90**	**5.81**	**5.73**	**6.90**	**4.63**	**6.51**	**7.05**	**8.80**	**12.7**	**190**	**206**	**174**	**203**
		2.05	*1.79*	*1.79*	*1.97*	*2.43*	*1.93*	*2.22*	*2.39*	*3.28*	*3.79*	*2.45*	*3.47*	*153*	*195*	*163*	*178*
	0.03	**2.38**	**2.11**	**2.11**	**2.64**	**2.69**	**2.55**	**3.43**	**2.33**	**2.66**	**3.08**	**3.87**	**5.61**	**179**	**203**	**160**	**183**
		0.86	*0.83*	*0.81*	*1.08*	*1.05*	*0.79*	*0.89*	*1.02*	*1.29*	*1.50*	*1.27*	*1.65*	*151*	*196*	*158*	*168*
	0.04	**1.46**	**1.46**	**1.36**	**1.59**	**1.76**	**1.70**	**2.23**	**1.47**	**1.68**	**1.96**	**2.34**	**3.28**	**87.7**	**199**	**108**	**178**
		0.66	*0.61*	*0.54*	*0.65*	*0.62*	*0.60*	*0.65*	*0.68*	*0.83*	*1.01*	*0.56*	*0.78*	*89.6*	*195*	*117*	*170*
	0.05	**1.08**	**1.08**	**1.08**	**1.22**	**1.31**	**1.24**	**1.63**	**1.12**	**1.27**	**1.33**	**1.69**	**2.23**	**23.4**	**197**	**84.1**	**189**
		0.28	*0.27*	*0.29*	*0.45*	*0.53*	*0.43*	*0.56*	*0.34*	*0.52*	*0.50*	*0.52*	*0.84*	*14.3*	*188*	*99.8*	*174*
mean	0.5	**32.1**	**16.0**	**13.5**	**13.0**	**13.7**	**14.7**	**17.9**	**13.5**	**12.0**	**12.6**	**15.0**	**18.3**	**191**	**180**	**192**	**179**
		21.6	*6.74*	*5.19*	*4.81*	*5.17*	*6.03*	*7.01*	*5.12*	*4.61*	*5.40*	*7.25*	*8.30*	*153*	*181*	*178*	*167*
	1	**4.98**	**3.70**	**3.59**	**3.52**	**3.55**	**3.71**	**4.79**	**3.59**	**3.34**	**3.29**	**3.63**	**4.87**	**133**	**79.6**	**174**	**187**
		1.51	*0.89*	*0.84*	*0.83*	*0.84*	*0.74*	*1.21*	*0.87*	*0.90*	*0.93*	*1.18*	*1.44*	*129*	*101*	*169*	*172*
	1.5	**2.70**	**1.91**	**1.89**	**1.88**	**1.87**	**1.87**	**2.55**	**1.91**	**1.88**	**1.84**	**1.87**	**2.56**	**18.2**	**28.2**	**153**	**153**
		0.61	*0.29*	*0.31*	*0.33*	*0.34*	*0.33*	*0.61*	*0.29*	*0.33*	*0.37*	*0.47*	*0.65*	*13.2*	*23.8*	*156*	*155*
	2	**1.89**	**1.00**	**1**	**1**	**1**	**1.01**	**1.75**	**1**	**1**	**1**	**1.19**	**1.72**	**8.38**	**13.7**	**141**	**134**
		0.32	*0.05*	*0*	*0*	*0*	*0.08*	*0.43*	*0*	*0*	*0*	*0.39*	*0.45*	*3.46*	*7.98*	*150*	*147*
	2.5	**1**	**1**	**1**	**1**	**1**	**1**	**1.01**	**1**	**1**	**1**	**1**	**1.15**	**5.40**	**8.93**	**118**	**118**
		0	*0*	*0*	*0*	*0*	*0*	*0.08*	*0*	*0*	*0*	*0*	*0.35*	*1.99*	*4.41*	*132*	*132*
	3	**1**	**1**	**1**	**1**	**1**	**1**	**1**	**1**	**1**	**1**	**1**	**1**	**3.96**	**6.80**	**90.4**	**97.9**
		0	*0*	*0*	*0*	*0*	*0*	*0*	*0*	*0*	*0*	*0*	*0*	*1.33*	*3.06*	*113*	*123*

Table 2. *OC* ***ARL*** and *SDRL* in detecting spike shifts and joint shifts when $m_0 = 100$ and $w = 0.1$.

		G=26 (FPCA)							G=16					G=1 (MFPCA)	Other methods		
	δ	R=1	R=2	R=3	R=6	R=8	R=10	R=26	R=1	R=2	R=3	R=6	R=16	R=1	MPCA	VPCA	UMPCA
spike	0.01	**46.9**	**19.4**	**16.5**	**21.5**	**21.5**	**26.9**	**32.7**	**17.2**	**15.1**	**18.1**	**23.0**	**23.0**	**197**	**220**	**201**	**184**
		36.6	*8.16*	*6.72*	*10.4*	*10.2*	*15.3*	*19.3*	*7.0*	*6.1*	*7.8*	*13.2*	*13.2*	*159*	*201*	*182*	*169*
	0.02	**5.28**	**4.22**	**3.83**	**4.47**	**4.44**	**4.91**	**6.59**	**3.87**	**3.63**	**4.00**	**4.63**	**4.63**	**196**	**204**	**203**	**205**
		1.44	*1.13*	*1.02*	*1.24*	*1.28*	*1.38*	*1.75*	*0.94*	*0.88*	*1.27*	*1.54*	*1.54*	*6.61*	*194*	*181*	*179*
	0.03	**2.75**	**1.97**	**1.88**	**2.31**	**2.29**	**2.53**	**3.45**	**1.89**	**1.84**	**1.89**	**2.45**	**2.45**	**204**	**211**	**195**	**186**
		0.57	*0.41*	*0.33*	*0.65*	*0.65*	*0.66*	*0.73*	*0.32*	*0.36*	*0.43*	*0.72*	*0.72*	*2.10*	*198*	*176*	*170*
	0.04	**1.87**	**1.55**	**1.34**	**1.62**	**1.64**	**1.72**	**2.01**	**1.28**	**1**	**1.43**	**1.69**	**1.69**	**192**	**202**	**193**	**182**
		0.34	*0.50*	*0.48*	*0.49*	*0.48*	*0.45*	*0.42*	*0.45*	*0*	*0.50*	*0.46*	*0.46*	*0.93*	*197*	*176*	*170*
	0.05	**1**	**1**	**1**	**1**	**1**	**1**	**1.74**	**1**	**1**	**1**	**1**	**1**	**175**	**217**	**203**	**181**
		0	*0*	*0*	*0*	*0*	*0*	*0.44*	*0*	*0*	*0*	*0*	*0*	*0.59*	*194*	*178*	*172*
joint	0.5	**195**	**191**	**190**	**200**	**196**	**191**	**165**	**183**	**173**	**190**	**84.0**	**71.4**	**171**	**218**	**185**	**188**
		163	*155*	*155*	*156*	*156*	*191*	*140*	*158*	*153*	*157*	*146*	*75.8*	*146*	*197*	*177*	*171*
	1	**36.2**	**19.8**	**17.8**	**21.6**	**22.0**	**25.1**	**26.6**	**10.2**	**12.0**	**27.4**	**7.7**	**10.3**	**94.5**	**169**	**181**	**203**
		22.3	*8.70*	*7.39*	*10.6*	*11.0*	*25.1*	*15.7*	*3.8*	*5.5*	*24.9*	*24.5*	*5.6*	*105*	*174*	*166*	*181*
	1.5	**8.46**	**6.91**	**6.51**	**6.30**	**5.91**	**6.25**	**8.69**	**3.90**	**4.38**	**2.47**	**2.58**	**4.06**	**25.9**	**118**	**153**	**182**
		2.66	*2.34*	*2.12*	*2.15*	*2.24*	*6.25*	*3.30*	*1.20*	*1.57*	*2.05*	*4.08*	*1.87*	*27.1*	*140*	*152*	*167*
	2	**4.42**	**3.40**	**2.68**	**2.03**	**1.83**	**2.10**	**3.94**	**1.87**	**1.58**	**1.01**	**1.02**	**1.78**	**6.47**	**66.4**	**110**	**180**
		1.35	*1.37*	*1.32*	*0.90*	*0.74*	*2.10*	*1.49*	*0.50*	*0.58*	*0.10*	*1.56*	*0.74*	*6.16*	*78.2*	*121*	*173*
	2.5	**1.73**	**1.02**	**1**	**1**	**1**	**1**	**1.76**	**1**	**1**	**1**	**1**	**1.01**	**1.37**	**37.1**	**72.8**	**183**
		1.02	*0.16*	*0*	*0*	*0*	*1*	*0.72*	*0*	*0.04*	*0*	*0.68*	*0.09*	*0.94*	*34.2*	*84.1*	*169*
	3	**1.02**	**1**	**1**	**1**	**1**	**1**	**1.01**	**1**	**1**	**1**	**1**	**1**	**1**	**20.6**	**50.5**	**177**
		0.13	*0*	*0*	*0*	*0*	*1*	*0.09*	*0*	*0*	*0*	*0.03*	*0*	*0*	*12.7*	*54.8*	*170*

Table 3. *OC* ***ARL*** and *SDRL* in detecting slope shifts and mean shifts when $m_0 = 100$ and $w = 0.05$.

		G=26 (FPCA)							G=16					G=1 (MFPCA)	Other methods		
	δ	R=1	R=2	R=3	R=6	R=8	R=10	R=26	R=1	R=2	R=3	R=6	R=16	R=1	MPCA	VPCA	UMPCA
IC	0	**204**	**197**	**201**	**202**	**201**	**202**	**201**	**198**	**203**	**199**	**196**	**198**	**202**	**201**	**201**	**202**
		158	165	164	164	175	174	182	167	168	165	163	156	158	199	186	180
slope	0.01	**12.4**	**9.42**	**11.8**	**13.9**	**17.1**	**15.4**	**20.6**	**11.6**	**18.5**	**22.5**	**27.7**	**38.7**	**190**	**204**	**195**	**198**
		6.55	4.85	*5.94*	*7.40*	*9.27*	*8.50*	10.9	*8.71*	*13.5*	*16.7*	*24.9*	*32.0*	*159*	*194*	*180*	*174*
	0.02	**3.78**	**3.35**	**3.33**	**3.68**	**3.90**	**4.83**	**6.39**	**2.98**	**4.13**	**4.15**	**5.10**	**6.90**	**96.6**	**202**	**165**	**195**
		1.67	*1.39*	*1.44*	*1.63*	*1.66*	*2.00*	*2.49*	*1.86*	*3.17*	*3.10*	*3.89*	*4.42*	*111*	*193*	*159*	*181*
	0.03	**1.93**	**1.66**	**1.69**	**2.03**	**2.10**	**2.14**	**3.09**	**1.41**	**1.94**	**2.04**	**2.04**	**2.72**	**11.6**	**208**	**117**	**191**
		0.73	*0.67*	*0.73*	*0.88*	*0.94*	*0.94*	*1.39*	*0.65*	*1.22*	*137*	*1.33*	*1.79*	*14.2*	*194*	*117*	*170*
	0.04	**1.13**	**1.12**	**1.18**	**1.39**	**1.66**	**1.47**	**1.80**	**1.08**	**1.26**	**1.30**	**1.61**	**1.98**	**6.45**	**197**	**69.4**	**175**
		0.37	*0.34*	*0.41*	*0.57*	*0.69*	*0.94*	*0.72*	*0.27*	*0.55*	*0.57*	*0.78*	*1.13*	*8.67*	*190*	*72.8*	*173*
	0.05	**1.04**	**1.02**	**1.10**	**1.15**	**1.16**	**1.28**	**1.33**	**1.03**	**1.03**	**1.11**	**1.13**	**1.37**	**3.36**	**189**	**45.5**	**174**
		0.06	*0.14*	*0.32*	*0.38*	*0.36*	*0.48*	*0.50*	*0.17*	*0.17*	*0.33*	*0.39*	*0.56*	*4.91*	*185*	*46.6*	*171*
mean	0.5	**13.0**	**10.0**	**9.51**	**9.60**	**9.74**	**9.83**	**12.2**	**12.3**	**10.4**	**10.0**	**11.4**	**13.9**	**176**	**121**	**94.4**	**185**
		6.30	*4.55*	*3.84*	*3.74*	*3.94*	*3.98*	*4.66*	*6.11*	*4.62*	*4.75*	*5.55*	*6.45*	*160*	*137*	*102.3*	*170*
	1	**3.87**	**3.14**	**2.78**	**2.74**	**2.83**	**2.90**	**3.62**	**3.54**	**3.28**	**3.03**	**3.26**	**3.91**	**150**	**39.7**	**27.3**	**180**
		1.33	*0.99*	*0.66*	*0.67*	*0.81*	*0.85*	*1.09*	*1.26*	*1.03*	*0.99*	*1.26*	*1.49*	*154*	*34.8*	*22.7*	*168*
	1.5	**1.87**	**1.81**	**1.80**	**1.73**	**1.73**	**1.67**	**1.84**	**1.81**	**1.78**	**1.72**	**1.76**	**2.09**	**82.5**	**18.5**	**13.0**	**130**
		0.34	*0.39*	*0.39*	*0.44*	*0.45*	*0.46*	*0.47*	*0.39*	*0.42*	*0.45*	*0.53*	*0.69*	*125*	*10.9*	*8.60*	*136*
	2	**1.40**	**1**	**1**	**1**	**1**	**1**	**1.33**	**1.19**	**1**	**1**	**1.16**	**1.53**	**23.4**	**11.5**	**8.17**	**107**
		0.49	*0*	*0*	*0*	*0*	*0*	*0.47*	*0.40*	*0*	*0*	*0.36*	*0.50*	*48.1*	*3.83*	*4.97*	*127*
	2.5	**1**	**1**	**1**	**1**	**1**	**1**	**1**	**1**	**1**	**1**	**1**	**1.04**	**11.5**	**7.87**	**5.38**	**89.5**
		0	*0*	*0*	*0*	*0*	*0*	*0*	*0*	*0*	*0*	*0*	*0.19*	*8.68*	*3.83*	*3.09*	*110*
	3	**1**	**1**	**1**	**1**	**1**	**1**	**1**	**1**	**1**	**1**	**1**	**1**	**8.03**	**5.67**	**4.31**	**66.3**
		0	*0*	*0*	*0*	*0*	*0*	*0*	*0*	*0*	*0*	*0*	*0*	*5.77*	*2.55*	*2.37*	*91.6*

Table 4. *OC* ***ARL*** and *SDRL* in detecting spike shifts and joint shifts when $m_0 = 100$ and $w = 0.05$.

		G=26 (FPCA)							G=16					G=1 (MFPCA)	Other methods		
	δ	R=1	R=2	R=3	R=6	R=8	R=10	R=26	R=1	R=2	R=3	R=6	R=16	R=1	MPCA	VPCA	UMPCA
spike	0.01	**14.4**	**10.8**	**10.6**	**10.9**	**11.8**	**12.4**	**16.2**	**11.5**	**10.1**	**10.8**	**13.2**	**16.3**	**12.9**	**199**	**206**	**192**
		7.03	*5.08*	*4.40*	*4.66*	*5.22*	*5.60*	*6.49*	*4.68*	*4.51*	*5.06*	*6.17*	*6.92*	*6.47*	*189*	*187*	*173*
	0.02	**4.21**	**3.30**	**3.14**	**3.26**	**3.40**	**3.60**	**4.70**	**3.18**	**3.06**	**3.16**	**3.64**	**4.47**	**3.96**	**192**	**201**	**198**
		1.33	*1.06*	*0.99*	*1.01*	*1.09*	*1.19*	*1.37*	*1.05*	*0.99*	*1.09*	*1.40*	*1.51*	*1.35*	*185*	*185*	*182*
	0.03	**2.11**	**1.77**	**1.73**	**1.74**	**1.74**	**1.78**	**2.48**	**1.79**	**1.77**	**1.72**	**1.84**	**2.43**	**2.12**	**191**	**198**	**190**
		0.60	*0.42*	*0.44*	*0.451*	*0.44*	*0.47*	*0.68*	*0.41*	*0.42*	*0.44*	*0.57*	*0.72*	*0.68*	*186*	*178*	*173*
	0.04	**1.65**	**1.01**	**1**	**1.01**	**1.18**	**1.33**	**1.72**	**1**	**1**	**1**	**1.38**	**1.67**	**1.53**	**202**	**197**	**187**
		0.48	*0.08*	*0*	*0.07*	*0.38*	*0.47*	*0.45*	*0*	*0*	*0*	*0.48*	*0.47*	*0.49*	*185*	*180*	*178*
	0.05	**1**	**1**	**1**	**1**	**1**	**1**	**1.05**	**1**	**1**	**1**	**1**	**1.10**	**1**	**196**	**189**	**179**
		0	*0*	*0*	*0*	*0*	*0*	*0.22*	*0*	*0*	*0*	*0*	*0.29*	*0*	*186*	*175*	*168*
joint	0.5	**153**	**111**	**120**	**116**	**121**	**116**	**105**	**158**	**134**	**34.6**	**100**	**108**	**148**	**178**	**196**	**195**
		145	*112*	*113*	*118*	*118*	*114*	*101*	*153*	*133*	*35.8*	*107*	*96.2*	*144*	*177*	*179*	*173*
	1	**13.4**	**10.9**	**10.9**	**9.6**	**11.8**	**12.1**	**14.7**	**10.6**	**11.2**	**5.59**	**12.8**	**15.0**	**31.7**	**111**	**164**	**199**
		6.06	*4.94*	*4.66*	*5.00*	*5.40*	*5.54*	*7.18*	*5.12*	*5.56*	*3.34*	*7.33*	*8.51*	*38.8*	*123*	*155*	*182*
	1.5	**6.29**	**5.00**	**4.81**	**4.16**	**4.11**	**4.02**	**5.75**	**4.30**	**4.41**	**1.91**	**4.59**	**6.03**	**8.44**	**57.9**	**110**	**192**
		2.45	*2.07*	*1.91*	*1.69*	*1.74*	*1.76*	*2.55*	*1.75*	*1.97*	*0.86*	*2.44*	*3.10*	*7.49*	*52.6*	*117*	*171*
	2	**3.26**	**2.11**	**1.54**	**1.36**	**1.31**	**1.34**	**2.30**	**2.27**	**1.94**	**1.65**	**1.97**	**2.88**	**2.94**	**30.4**	**67.4**	**177**
		1.44	*1.13*	*0.82*	*0.47*	*0.48*	*0.51*	*1.04*	*0.72*	*0.65*	*0*	*0.89*	*1.40*	*2.61*	*18.8*	*72.3*	173
	2.5	**1.14**	**1.01**	**1**	**1**	**1**	**1**	**1.12**	**1.08**	**1**	**1**	**1.02**	**1.48**	**1.11**	**20.5**	**45.4**	**180**
		0.41	*0.12*	*0*	*0*	*0*	*0*	*0.32*	*0.27*	*0*	*0*	*0.14*	*0.59*	*0.41*	*10.5*	*49.5*	*170*
	3	**1**	**1**	**1**	**1**	**1**	**1**	**1**	**1**	**1**	**1**	**1**	**1**	**1**	**14.4**	**30.6**	**164**
		0	*0*	*0*	*0*	*0*	*0*	*0*	*0*	*0*	*0*	*0*	*0*	*0*	*6.83*	*25.1*	*166*

7. References

Ding, Y.; Zeng, L.; and Zhou, S. (2006). "Phase I Analysis for Monitoring Nonlinear Profiles in Manufacturing Processes". *Journal of Quality Technology* 38(3), pp. 199.

Eyvazian, M., Noorossana, R., Saghaei, A., and Amiri, A. (2011). "Phase II monitoring of multivariate multiple linear regression profiles. *Quality and Reliability Engineering International* 27(3), pp. 281-296.

Ghashghaei, R., and Amiri, A. (2016). "Sum of Squares Control Charts for Monitoring of Multivariate Multiple Linear Regression Profiles in Phase II". Published online in *Quality and Reliability Engineering International.* doi: 10.1002/qre.2055.

Grasso, M.; Colosimo, B.M.; and Pacella, M. (2014). "Profile Monitoring via Sensor Fusion: The Use of PCA Methods for Multi-Channel Data". *International Journal of Production Research* 52(20), pp. 6110–6135.

Jackson, J. E.; and Mudholkar, G.S. (1979). "Control Procedures for Residuals Associated with Principal Component Analysis". *Technometrics* 21(3), pp. 341–349.

Jensen, W. A.; Birch, J.B.; and Woodall, W.H. (2008). "Monitoring Correlation Within Linear Profiles Using Mixed Models". *Journal of Quality Technology* 40(2), pp. 167–183.

Jin, J.; and Shi, J. (1999). "Feature-Preserving Data Compression of Stamping Tonnage Information Using Wavelets". *Technometrics* 41(4), pp. 327-339.

Jin, J.; and Shi, J. (2001). "Automatic Feature Extraction of Waveform Signals for in-Process Diagnostic Performance Improvement". *Journal of Intelligent Manufacturing* 12(3), pp. 257–268.

Keogh, E.; and Ratanamahatana, C.A. (2005). "Exact Indexing of Dynamic Time Warping". *Knowledge and Information Systems* 7(3), pp. 358–386.

Kim, J.; Huang, Q.; Shi, J.; and Chang, T. S. (2006)."Online Multichannel Forging Tonnage Monitoring and Fault Pattern Discrimination Using Principal Curve". *Journal of Manufacturing Science and Engineering,* 128(4), pp. 944-950.

Lee, S. P.; Chao, A. K.; Tsung, F.; Wong, D. S. H.; and Tseng, S.T. (2011). "Monitoring Batch Processes with Multiple on-off Steps in Semiconductor Manufacturing". *Journal of Quality Technology* 43(2), pp. 142–157.

Liu, K.; Mei, Y.; and Shi, J. (2015). "An Adaptive Sampling Strategy for Online High-Dimensional Process Monitoring". *Technometrics* 57(3), pp. 305–319.

Mahmoud, M. A.; and Woodall, W.H. (2004). "Phase I Analysis of Linear Profiles With Calibration Applications". *Technometrics* 46(4), pp. 380–391.

Mei, Y. (2010). "Efficient Scalable Schemes for Monitoring a Large Number of Data Streams. *Biometrika* 97(2), pp. 419–433.

Mei, Y. (2011). "Quickest Detection in Censoring Sensor Networks". In *Information Theory Proceedings (ISIT)*, *2011 IEEE International Symposium on* (pp. 2148–2152). IEEE.

Nomikos, P. and MacGregor, J. F. (1995). "Multivariate SPC charts for monitoring batch processes". *Technometrics*, 37(1), pp. 41-59.

Noorossana, R., Eyvazian, M., and Vaghefi, A. (2010). "Phase II monitoring of multivariate simple linear profiles". *Computers & Industrial Engineering*, 58(4), pp. 563-570.

Noorossana, R.; Eyvazian, M.; Amiri, A.; and Mahmoud, M. A. (2010). "Statistical Monitoring of Multivariate Multiple Linear Regression Profiles in Phase I with Calibration Application". *Quality and Reliability Engineering International* 26(3), pp. 291–303.

Noorossana, R., Saghaei, A., and Amiri, A. (2011). Statistical analysis of profile monitoring (Vol. 865). John Wiley & Sons.

Paynabar, K.; and Jin, J. (2011). "Characterization of Non-Linear Profiles Variations Using Mixed-Effect Models and Wavelets". *IIE Transactions* 43(4), pp. 275–290.

Paynabar, K.; Jin, J.; and Pacella, M. (2013). "Monitoring and Diagnosis of Multichannel Nonlinear Profile Variations Using Uncorrelated Multilinear Principal Component Analysis". *IIE Transactions* 45(11), pp. 1235–1247.

Paynabar, K.; Qiu, P.; and Zou, C. (2015). "A Change Point Approach for Phase-I Analysis in Multivariate Profile Monitoring and Diagnosis". *Technometrics* 58(2), pp. 191–204.

Qiu, P.; Zou, C.; and Wang, Z. (2010). "Nonparametric Profile Monitoring by Mixed Effects Modeling". *Technometrics* 52(3), pp. 265-277.

Tartakovsky, A. G.; Rozovskii, B. L.; Blažek, R. B.; and Kim, H. (2006). "Detection of Intrusions in Information Systems by Sequential Change-Point Methods". *Statistical Methodology* 3(3), pp. 252–293.

Thorndike, R. L. (1953). "Who Belongs in the Family?". *Psychometrika*. 18 (4), pp. 267–276.

Tibshirani, R.; Walther, G.; and Hastie, T. (2001) "Estimating the Number of Clusters in a Dataset via the Gap Statistic," *Journal of the Royal Statistical Society, Series B*, 63, pp. 411–423.

Walker, E.; and Wright, S. P. (2002). "Comparing Curves Using Additive Models". *Journal of Quality Technology* 34(1), pp. 118.

Woodall, W. H. (2007). "Current Research on Profile Monitoring". *Production* 17(3), pp. 420–425.

Yu, G.; Zou, C.; and Wang, Z. (2012). "Outlier Detection in Functional Observations With Applications to Profile Monitoring". *Technometrics* 54(3), pp. 308–318.

Zhang, C.; Chen, N.; and Zou, C. (2016). "Robust Multivariate Control Chart Based on Goodness-of-Fit Test". *Journal of Quality Technology* 48(2), pp. 139.

Zhou, S.; Sun, B.; and Shi, J. (2006). "An SPC Monitoring System for Cycle-Based Waveform Signals Using Haar Transform". *Automation Science and Engineering, IEEE Transactions on* 3(1), pp. 60–72.

Zou, C.; Ning, X.; and Tsung, F. (2012). "LASSO-Based Multivariate Linear Profile Monitoring". *Annals of Operations Research* 192(1), pp. 3–19.

Zou, C.; Tsung, F.; and Wang, Z. (2007). "Monitoring General Linear Profiles Using Multivariate Exponentially Weighted Moving Average Schemes". *Technometrics* 49(4), pp. 395–408.

Zou, C.; Tsung, F.; and Wang, Z. (2008). "Monitoring Profiles Based on Nonparametric Regression Methods". *Technometrics* 50(4), pp. 512–526.